Analytical and Experimental Study of Vibrating Rectangular Plates on Rigid Point Supports

D.J. Gorman*
University of Ottawa, Ottawa, Canada K1N 6N5
and
R.K. Singal†
Canadian Space Agency, Ottawa, Canada K2H 8S2

An analytical-type solution based on the superposition method is developed for the free-vibration frequencies and mode shapes of rectangular plates resting on arbitrarily located rigid point supports. The supports are of the type realized by means of bolts or spot welds. An extensive experimental program was conducted in support of the project, and excellent agreement between computed and experimental results was obtained. While the analysis is general in nature, it will be highly applicable to the study of vibration of electronic circuit boards and solar panels.

Nomenclature

a,b	= dimensions of plate
D	= plate flexural rigidity, $= Eh^3/12(1-\nu^2)$
E	= Young's modulus of plate material
h	= plate thickness
k	= number of terms used in series expansions
k^*	= upper limit for number of terms in first summation
M	= amplitude of applied bending moment
Mb^2/aD	= dimensionless bending moment
M_R	= ratio of attached mass to total mass of plate
N	= total number of discrete point supports acting on plate
P	= amplitude of concentrated force
P^*	= dimensionless concentrated force amplitude, $= -2Pb^3/Da^2$
u	= distance to point support in ξ direction divided by a
U	= dimensionless distance to center point of rigid point support
v	= distance to point support in η direction divided by b
ν^*	$= 1-\nu$
W	= plate lateral displacement amplitude divided by dimension a
λ^2	= plate free-vibration eigenvalue, $= \omega a^2\sqrt{\rho/D}$
η	= distance along plate coordinate divided by b
ν	= Poisson's ratio of plate material
ξ	= distance along plate coordinate divided by a
ρ	= mass of plate per unit area
ϕ	= plate aspect ratio, $= b/a$
ω	= circular frequency of plate vibration

Introduction

NUMEROUS papers have appeared in the literature in recent years dealing with the free-vibration analysis of point-supported rectangular plates.[1-7] Many of these papers provide a detailed review of the literature up to the time of their publication. The investigation of Leuner[7] involves a study of the free vibration of rectangular plates with elastic point supports at the corners. It is somewhat unique in that it involves a rather extensive experimental program. The work to be presented here constitutes a logical extension of earlier work published by the first author.[2,3]

The objective of this work is to address not only problems of the type encountered in analysis of the dynamics of rectangular solar panels, for example, but also problems of strong current interest related to the fatigue life of rectangular electronic circuit boards. In its most general application, the analysis described here permits the obtaining of analytical-type solutions for the free-vibration frequencies and mode shapes of thin rectangular plates supported at any number of discrete points. It is shown how the theory is easily modified to handle the same plates with any number of discrete attached masses. The point supports may be located at any arbitrarily designated locations on the plate lateral surface. They may be of the simplest type where plate lateral displacement is forbidden but rotation is permitted, or they may be of the type where both displacement and rotation are forbidden. This latter type of support is to be expected where threaded screws or welds are used to attach the plate to small circular base supports. It is realized in the present analysis by the use of clusters of point supports to be discussed later. Attached masses could be of any magnitude and have any desired coordinate position on the plate lateral surface. All solutions are obtained by means of the superposition method as developed by the first author and described in earlier publications.[8] An extensive experimental program has been undertaken to confirm the validity of the approach.

Development of the Mathematical Model

In Ref. 3, a detailed description of the mathematical procedure for conducting a free-vibration analysis of the completely free plate with four symmetrically distributed point supports was provided. The superposition method was employed and, taking advantage of symmetry, the problem was simplified by reducing it to the analysis of three mode families. In fact, only one quarter of the plate had to be analyzed. The mode families consisted of modes that were completely symmetric with respect to the plate central axes, modes completely antisymmetric with respect to these axes, and modes symmetric with respect to one axis and antisymmetric with respect to the other.

In the present work, no restrictions with respect to symmetry are imposed. The first part of the analysis relating to the completely free rectangular plate follows almost exactly the same path as that described earlier for the fully symmetric

Received Oct. 11, 1989; revision received March 16, 1990.

*Professor, Department of Mechanical Engineering.
†Research Scientist, Directorate of Space Mechanics, 3701 Carling Ave., P.O. Box 11490, Station H.

modes in Ref. 3. The reader may wish to review this reference since the details reported earlier will not be repeated here.

Analysis for the Completely Free Plate

This part of the analysis is achieved with the building blocks of Fig. 1. Each building block is of the type used in the analysis of the fully symmetric modes of Ref. 3. The only significant difference is that now each block encompasses the entire plate instead of the quarter plate as was the case earlier. Except along the driven edge, each edge of each block is given slip shear boundary conditions, i.e., vertical edge reaction along the edge, and slope taken normal to the edge, is everywhere zero. This condition is represented in the figure by two small circles adjacent to the edge. Vertical edge reaction is also forbidden along each driven edge, the edge itself being driven by a distributed harmonic bending moment or edge rotation of circular frequency ω.

Only the solution for the first building block is provided here. The solution for plate lateral displacement can be written in the form proposed by Lévy as

$$W_1(\xi,\eta) = \sum_{m=0,1}^{\infty} Y_m(\eta) \cos m\pi\xi \tag{1}$$

Because of boundary conditions imposed along the edge, $\eta = 0$, hyperbolic sine and sine functions normally appearing in the functions $Y_m(\eta)$ must be deleted.

Representing the amplitude of the driving bending moment distributed along the edge, $\eta = 1$, as

$$\frac{Mb^2}{aD} = \sum_{m=0,1}^{\infty} E_m \cos m\pi\xi \tag{2}$$

and enforcing the conditions of zero vertical edge reaction and moment equilibrium along this edge, it is easily shown that we obtain[3]

$$W^1(\xi,\eta) = \sum_{m=0,1}^{k^*} E_m\left(\theta_{11m}\frac{\cosh\beta_m\eta}{\sinh\beta_m} + \theta_{13m}\frac{\cos\gamma_m\eta}{\sin\gamma_m}\right)\cos m\pi\xi$$

$$+ \sum_{m=k^*+1}^{\infty} E_m\left(\theta_{22m}\frac{\cosh\beta_m\eta}{\sinh\beta_m} + \theta_{23m}\frac{\cosh\gamma_m\eta}{\sinh\gamma_m}\right)\cos m\pi\xi \tag{3}$$

where

$$\beta_m = \phi\sqrt{\lambda^2 + (m\pi)^2}$$

and

$$\gamma_m = \phi\sqrt{\lambda^2 - (m\pi)^2}, \quad \text{or} \quad \phi\sqrt{(m\pi)^2 - \lambda^2}$$

whichever is real, and the first summation contains only terms for which $\lambda^2 > (m\pi)^2$. The quantities θ_{11m} and θ_{22m}, etc., are easily determined functions of the other parameters.

It will be obvious that solutions for the other three building blocks are readily extracted from that provided for the first one. It is only a question of properly interchanging the variables η and ξ. Before turning our attention to the generation of the eigenvalue matrix, we will look next at the other types of building blocks required.

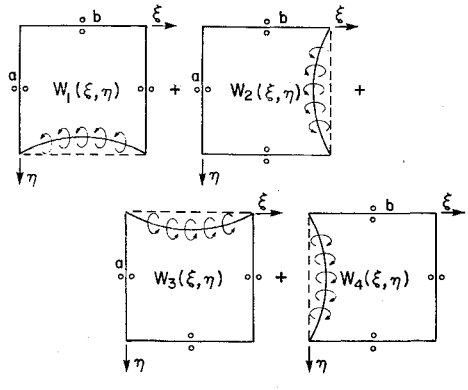

Fig. 1 First four building blocks used in analysis of rigid point-supported plates. These blocks by themselves permit the analysis of the completely free plate.

Building Blocks Driven by a Harmonic Point Force

This building block is shown schematically in Fig. 2. Slip shear boundary conditions are imposed along all the external edges, and a concentrated harmonic driving force P^* is applied at the coordinates u and v. The spatial distribution of the plate displacement is represented by two different functions $W_{51}(\xi,\eta)$ and $W_{52}(\xi,\eta)$, in the regions I and II, respectively, as indicated in the figure. These Lévy-type solutions are arrived at by enforcing the appropriate boundary conditions at the outer edges of the building block and enforcing the conditions of continuity and dynamic equilibrium across the common boundary between the two regions.[3] The amplitude of the concentrated force is represented by the Dirac function.

A detailed description of the development of the two solutions is provided in Ref. 3. It is sufficient therefore to provide here only the solutions as follows:

$$W_{51}(\xi,\eta) = \sum_{m=0,1}^{k^*} (A_m \cosh\beta_m\eta + B_m \cos\gamma_m\eta)\cos m\pi\xi$$

$$+ \sum_{m=k^*+1}^{\infty} (A_m \cosh\beta_m\eta + B_m \cosh\gamma_m\eta)\cos m\pi\xi \tag{4}$$

and

$$W_{52}(\xi,\eta) = \sum_{m=0,1}^{k^*} (C_m \cosh\beta_m\eta + D_m \cos\gamma_m\eta)\cos m\pi\xi$$

$$+ \sum_{m=k^*+1}^{\infty} (C_m \cosh\beta_m\eta + D_m \cosh\gamma_m\eta)\cos m\pi\xi \tag{5}$$

where β_m and γ_m are as defined earlier, and again the first summation contains only those terms for which $\lambda^2 > (m\pi)^2$.

Values for the coefficients A_m, B_m, etc., are as follows[8]:
For $\lambda^2 > (m\pi)^2$,

$$A_m = \frac{P^* \cos m\pi u \cosh\beta_m v^*}{\delta_m(\beta_m^2 + \gamma_m^2)\beta_m \sinh\beta_m}$$

$$B_m = \frac{P^* \cos m\pi u \cos\gamma_m v^*}{\delta_m(\beta_m^2 + \gamma_m^2)\gamma_m \sin\gamma_m}$$

$$C_m = \frac{P^* \cos m\pi u \cosh\beta_m v}{\delta_m(\beta_m^2 + \gamma_m^2)\beta_m \sinh\beta_m}$$

$$D_m = \frac{P^* \cos m\pi u \cos\gamma_m v}{\delta_m(\beta_m^2 + \gamma_m^2)\gamma_m \sin\gamma_m}$$

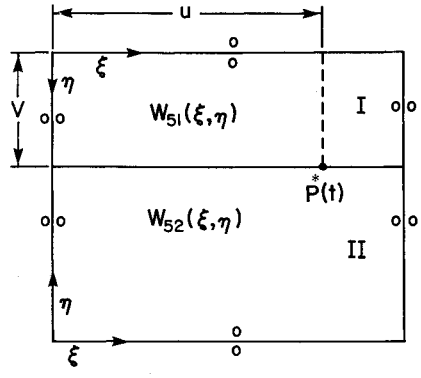

Fig. 2 Building block with harmonic concentrated driving force $P^*(t)$ located at coordinates u and v.

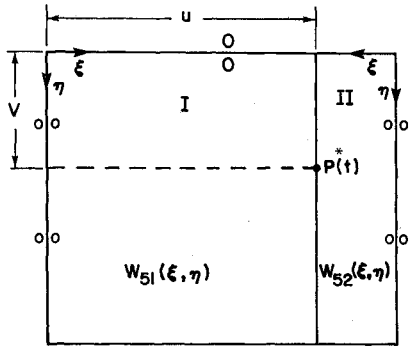

Fig. 3 Alternate representation of building block with harmonic concentrated driving force $P^*(t)$ located at coordinates u and v.

and for $\lambda^2 < (m\pi)^2$,

$$A_m = \frac{P^* \cosh m\pi u \cosh\beta_m v^*}{\delta_m(\beta_m^2 - \gamma_m^2)\beta_m \sinh\beta_m}$$

$$B_m = \frac{-P^* \cos m\pi u \cosh\gamma_m v^*}{\delta_m(\beta_m^2 - \gamma_m^2)\beta_m \sinh\gamma_m}$$

$$C_m = \frac{P^* \cos m\pi u \cosh\beta_m v}{\delta_m(\beta_m^2 - \gamma_m^2)\beta_m \sinh\beta_m}$$

$$D_m = \frac{-P^* \cos m\pi u \cosh\gamma_m v}{\delta_m(\beta_m^2 - \gamma_m^2)\gamma_m \sinh\gamma_m}$$

where $\delta_m = 2$, $m = 0$; $\delta_m = 1$, $m \neq 0$, and P^* is the amplitude of the dimensionless driving force.

It is highly advantageous to have a solution available for the preceding building block, where the block segments are as shown in Fig. 3.[3] Fortunately, this solution is easily extracted from the preceding solution through an appropriate interchange of coordinates. Referring to Fig. 3 and using subscript n to avoid confusion, it follows that we may write,

$$W_{52}(\xi,\eta) = \sum_{n=0,1}^{k^*} (C_n \cosh\beta_n\xi + D_n \cos\gamma_n\xi) \cos n\pi\eta + \sum_{n=k^*+1}^{\infty} (C_n \cosh\beta_n\xi + D_n \cosh\gamma_n\xi) \cos n\pi\eta \qquad (6)$$

where $\beta_n = (1/\phi)\sqrt{\lambda^2\phi^2 + (n\pi)^2}$, $\gamma_n = (1/\phi)\sqrt{\lambda^2\phi^2 - (n\pi)^2}$ or $(1/\phi)\sqrt{(n\pi)^2 - \lambda^2\phi^2}$, whichever is real, and the first summation contains only terms for which $\lambda^2\phi^2 \geq (n\pi)^2$. Following transformation rules as discussed in Ref. 8, we write:
For $\lambda^2\phi^2 > (n\pi)^2$

$$C_n = \frac{P^* \cos n\pi v \cosh\beta_n u}{(\beta_n^2 + \gamma_n^2)\beta_n\phi^4 \sinh\beta_n}$$

$$D_n = \frac{P^* \cos n\pi v \cos\gamma_n u}{(\beta_n^2 + \gamma_n^2)\gamma_n\phi^4 \sin\gamma_n}$$

and for $\lambda^2\phi^2 < (n\pi)^2$

$$C_n = \frac{P^* \cos n\pi v \cosh\beta_n u}{(\beta_n^2 - \gamma_n^2)\beta_n\phi^4 \sinh\beta_n}$$

$$D_n = \frac{-P^* \cos n\pi v \cosh\gamma_n u}{(\beta_n^2 - \gamma_n^2)\gamma_n\phi^4 \sinh\gamma_n}$$

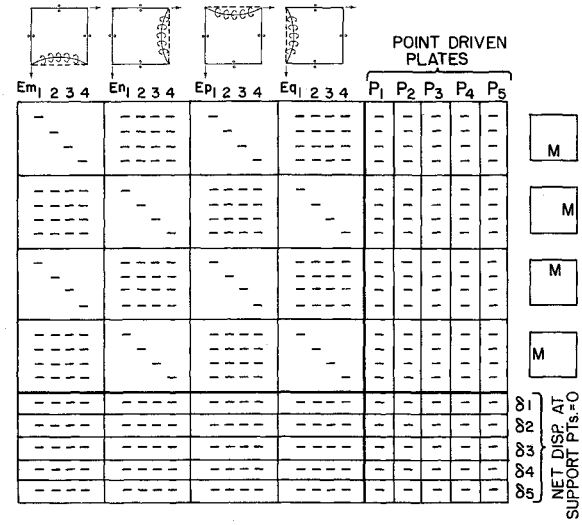

Fig. 4 Schematic representation of eigenvalue matrix that is constructed for analyzing rectangular plates with multipoint support.

The companion solution $W_{51}(\xi,\eta)$ can easily be extracted from the preceding solution.

We next focus attention on building blocks similar to that just discussed but with the concentrated driving force replaced by a concentrated inertia force resulting from a localized mass attached to the plate. Let a mass M_i be attached at the coordinates u_i, v_i.

The amplitude of the harmonic force exerted on the plate as a result of the inertia of the attached mass will be given by

$$P = M_i\omega^2 a W(u_i, v_i) \qquad (7)$$

Returning to the dimensionless form of the driving force we obtain, since by definition

$$P^* = \frac{-2Pb^3}{Da^2}$$

$$P^* = \frac{-2b^3}{Da} M_i\omega^2 W(u_i, v_i) \qquad (8)$$

But from the definition of the eigenvalue λ^2 we obtain $\omega^2 = \lambda^4 D/a^4\rho$, and introducing the mass ratio $M_{R_i} = M_i/\rho ab$, it is found that Eq. (8) may be expressed as

$$P^* = -2\phi^4 M_{R_i}\lambda^4 W(u_i, v_i) \qquad (9)$$

Using Eq. (9) for the quantity P^*, the solution for the building block with the attached mass will be identical to that provided earlier for the building block driven by the concentrated harmonic force.

Generation of the Eigenvalue Matrix

Consider first the analysis of a rectangular plate resting on N discrete point supports, each of which forbids lateral displacement of the plate at the point of application but imparts no bending moment to the plate. A schematic representation of the matrix that must be generated to analyze this problem is provided in Fig. 4. For illustrative purposes we have assumed the number of discrete point supports N to equal five, but of course N can take on any value we choose.

We begin by examining the portion of the matrix lying above and to the left of the heavy internal grid lines. This portion, taken by itself, would permit establishment of the eigenvalues of the completely free plate. It is generated in a manner identical to that described in Ref. 3. The upper segment of this portion is obtained by expanding the contribution

of each of the four primary building blocks to moment along the boundary, $\eta = 1$, in a cosine series. The net coefficient of each term would have to be set equal to zero if an analysis of the completely free plate was being conducted. This would lead to k simultaneous homogenous algebraic equations for the constants E_m, E_n, etc., associated with these building blocks. For illustrative purposes k, the number of terms in the primary building blocks series of Fig. 4, is taken to be equal to 4. Moving down through this portion of the matrix, we would obtain three other sets of equations resulting from the requirement of zero net bending moment along the other three edges of the plate as indicated on the small rectangles to the right of the figure. This portion of the matrix would, of itself, permit the obtaining of all free-vibration frequencies and mode shapes of the completely free rectangular plate with no restrictions as to whether the modes were fully symmetric or fully antisymmetric, etc., with respect to the plate central axis.

The object of our study here, however, goes beyond the completely free plate, and we must incorporate the effects of the point-driven building blocks into the analysis. We next focus our attention on the portion of the matrix above and to the right of the heavy grid lines. There will be one column in this portion associated with each of the point-driven plate solutions. Again, the elements in these columns represent the contribution of the plate solution to the appropriate Fourier component in the expansion of the bending moment indicated at the right-hand side of the matrix. it should be recalled that the form of each of the point-driven plate solutions is identical, with only the coordinates u and v varying from point to point. It will be evident that setting up these coordinates as u_i and v_i, with i varying from 1 to N, the number of point supports acting on the plate, a simple computer algorithm generates all of this portion of the matrix regardless of the value of N.

We turn next to the portion of the matrix below and to the left of the heavy grid lines. Each element in this portion of the matrix is set equal to the contribution of the associated primary building block to net displacement at the coordinates u_i and v_i related to the plate support indicated at the right-hand side of the matrix. Again, a simple computer algorithm generates this entire portion of the matrix.

Finally, we focus attention on the remaining portion of the matrix, below and to the right of the heavy grid lines. Each element here represents the displacement contribution of the associated point-driven plate solutions to the related point on the plate of interest. It will be appreciated that each of these elements, unlike the earlier elements, is obtained by conducting a summation of the contributions to the plate displacement of the various Fourier components used in representing the concentrated driving forces. Again, a simple computer algorithm is easily set up to generate this portion of the matrix.

We next address the problem of incorporating the effects of adding an attached mass to the plate at some coordinate position u, v that does not coincide with a plate point support. Let us suppose, for example, that instead of a point support at the coordinates u_5, v_5 associated with the last column of the matrix (Fig. 4), we have a mass attached to the plate with mass ratio equal M_{R5}. The quantity P_5^* now represents the driving force acting on the plate as a result of the inertia of the attached mass.

The net plate displacement $W(u_5,v_5)$ is represented by the summation of all of the elements in the final row of the matrix as presently constituted. From Eq. (9) it is evident that this summation is equal to $P_5^* Q_5$ where

$$Q_5 = \frac{-1}{2\phi^4 M_{R5} \lambda^4} \tag{10}$$

Satisfaction of the dynamic equilibrium equation at the location u_5, v_5 is ensured by simply subtracting the quantity Q from the final element in the lower right-hand side of the matrix.

In the general analysis, the procedure to be employed is as follows. Generate the eigenvalue matrix as though all points of interest on the plate, whether they are locations of point support or an attached mass, are in fact locations of point support. Let us denote the subscript "i" the building block with attached mass of mass ratio M_{R_i}, then locate the element i, i in the lower right-hand portion of this matrix where subscript i is measured from the intersection of the heavy grid lines. Subtract from this element the quantity Q_i as defined in Eq. (10). Make this post modification to the matrix for each pair of coordinates where there is an attached mass. Construction of the eigenvalue matrix is now complete.

Establishment of Eigenvalue and Mode Shapes

Eigenvalues and mode shapes are established in a manner identical to the described in earlier reports. A trial eigenvalue is selected, and the determinant of the associated matrix is obtained. The trial eigenvalue is then augmented, and the process is repeated until a change in sign of the determinant is obtained. One then moves in upon the actual eigenvalue, for which the determinant vanishes. Mode shapes are obtained by setting one of the unknown coefficients, E_M, P_i^*, etc., equal to unity and solving the resulting set of nonhomogenous equations for the remaining coefficients to obtain the mode shape.

The number of terms used in constructing the primary building blocks can be increased to achieve the desired convergence. It will be observed that the size of the matrix will always be $4k + N$ by $4k + N$. While more than k terms can be used in representing the Dirac functions for the solutions with concentrated driving forces or attached masses, without increasing the size of the matrix, experience has indicated that using k terms for these later expansions is quite satisfactory for problems explored here.

Theoretical and Experimental Results

It will appreciated that the array of problems that can be analyzed following the technique described here is so vast that no general tabulation of eigenvalues is possible. In addition to variation in plate aspect ratio, there exists an infinity of possible dispositions of plate lateral point supports and mass attachments. Accordingly, computed and experimental results presented and discussed here will be confined to those related to two rectangular aluminum plates of 10.0 in. (25.4 cm) by 15.0 in. (38.1 cm), of 0.0625 in. (1.59 mm) thickness as shown schematically in Fig. 5a and 5b. These plates are referred to herein as plate A and plate B, respectively. Plate A is given rigid point support at four locations along its diagonals, the locations being symmetrically distributed with respect to the plate central axis. Plate B is given rigid point support at four points lying along lines running parallel to the longer edges and one quarter of the way in from these edges. Again, the point supports are symmetrically distributed with respects to the plate central axis.

Eigenvalues are computed for the preceding plates based on rigid point support being provided in each case by conventional bolts or studs bearing on 5/8 in. (1.59 cm) diam circular washers. A relationship between the plate geometry and that of the support area is thereby established.

Achievement of "rigid support" at any desired location on the plate surface is realized in the computations by following steps similar to those described in Ref. 9. Four discrete point supports are brought to act at each support location at the extremities of the mutually perpendicular diameters of the washer as indicated schematically in Fig. 5. By demanding zero lateral displacement of the plate at each of these four points, a condition of essentially rigid support is achieved. The effect of the four discrete point supports is to eliminate lateral displacement as well as rotation of the plate at the location of interest. It would be easy to add a fifth discrete point support

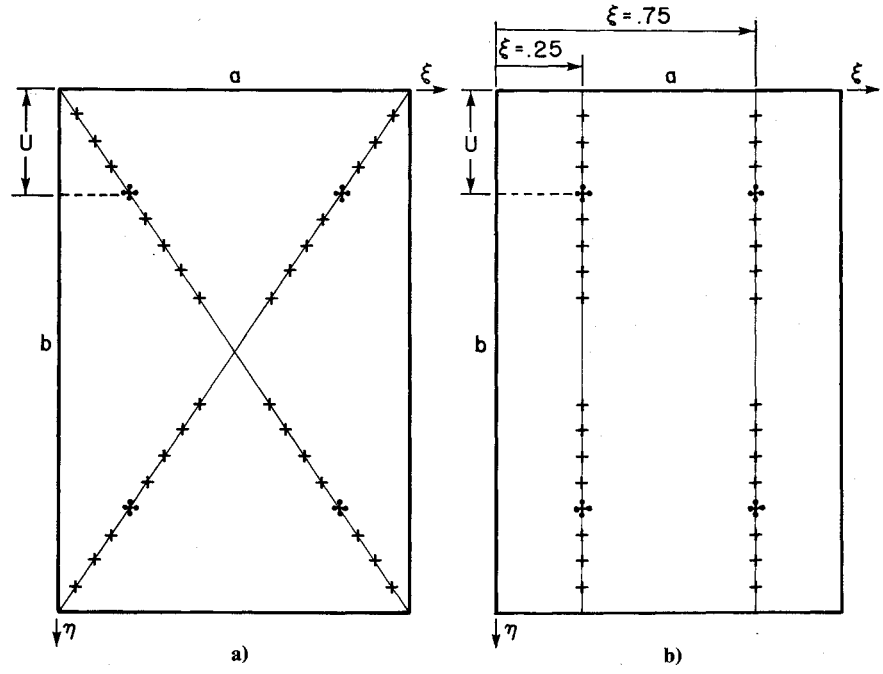

Fig. 5 Schematic representation of rectangular aluminum plates for which theoretical and experimental studies have been performed. Crosses indicate selected locations where rigid support points could be applied. Only four rigid supports at distance U from the edges are applied during a test.

Table 1 Computed and measured frequencies, Hz, for first four modes of free vibration of rectangular aluminum plate with four rigid point supports symmetrically distributed along diagonals [Fig. 5(a)]. Experimental values in bracket

	Modes			
U	1	2	3	4
0.05	54.9 (55.8)	92.9 (92.5)	136.0 (140.0)	154.0 (152.9)
0.10	75.6 (75.3)	114.0 (112.8)	180.0 (182.1)	181.0 (192.2)
0.15	102.0 (101.2)	138.0 (134.4)	203.0 (205.6)	224.0 (223.6)
0.20	138.0 (135.6)	167.0 (165.4)	188.0 (180.7)	192.0 (196.7)
0.25	127.0 (129.6)	131.0 (132.5)	160.0 (158.4)	162.0 (164.8)
0.30	90.8 (92.4)	92.4 (93.4)	116.0 (114.8)	116.0 (119.8)
0.35	66.9 (65.7)	67.5 (66.0)	86.9 (87.4)	87.3 (89.9)
0.40	50.4 (49.4)	51.4 (51.0)	68.0 (68.7)	68.4 (71.9)

Table 2 Computed and measured frequencies, Hz, for first four modes of free vibration of rectangular aluminum plate with four rigid point supports symmetrically distributed about plate central axis [Fig. 5(b)]. Experimental values in brackets

	Modes			
U	1	2	3	4
0.05	65.0 (62.0)	82.0 (77.4)	173.0 (176.1)	175.0 (169.9)
0.10	82.0 (81.5)	98.7 (96.4)	186.0 (191.9)	217.0 (214.0)
0.15	105.0 (104.2)	120.0 (120.7)	201.0 (209.1)	266.0 (261.7)
0.20	137.0 (133.4)	150.0 (150.3)	195.0 (185.7)	199.0 (184.0)
0.25	127.0 (129.6)	131.0 (132.5)	160.0 (158.4)	162.0 (164.8)
0.30	92.0 (89.4)	93.6 (90.6)	127.0 (123.8)	127.0 (125.8)
0.35	68.8 (67.3)	70.0 (67.8)	104.0 (99.8)	104.0 (100.3)
0.40	53.3 (55.6)	54.3 (56.6)	87.4 (84.3)	87.9 (87.3)

at the center of the washer area, but experience has indicated that this has little effect on the computed eigenvalues.

In Tables 1 and 2, the first four free-vibration frequencies, based on computed eigenvalues, are tabulated for plates A and B with rigid supports located at various dimensionless distances from the plate outer edges. Experimentally measured frequencies for the same plates are also presented.

In Figs. 6 and 7, first mode experimentally measured frequencies are compared in graphical form with those obtained theoretically, with support locations at various distances from the plate edges.

A photograph of a typical plate with the four rigid supports is provided in Fig. 8. The objective of the experimental study was to establish resonant frequencies and the associated mode shapes for the two sets of plates A and B. For this purpose, the method of impact testing was adopted. Fifty-five measurement point locations were chosen. Only one accelerometer was used; it was fixed at one suitable location, which was an antinode for the first four modes. The impact hammer was moved from one measurement point to another. For each measurement point, a frequency response function was obtained from the average of five impacts.

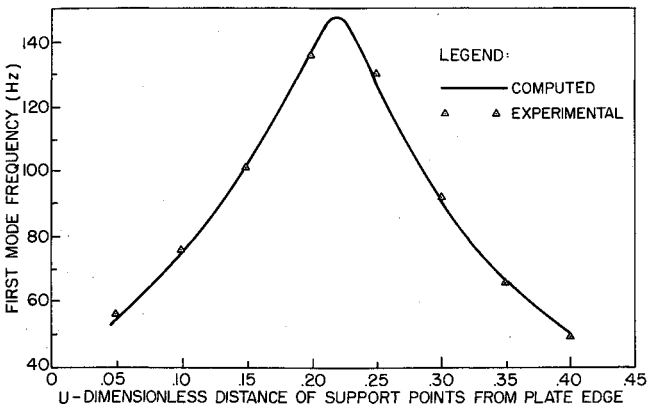

Fig. 6 Comparison of first mode computed and experimentally measured frequencies for plate A.

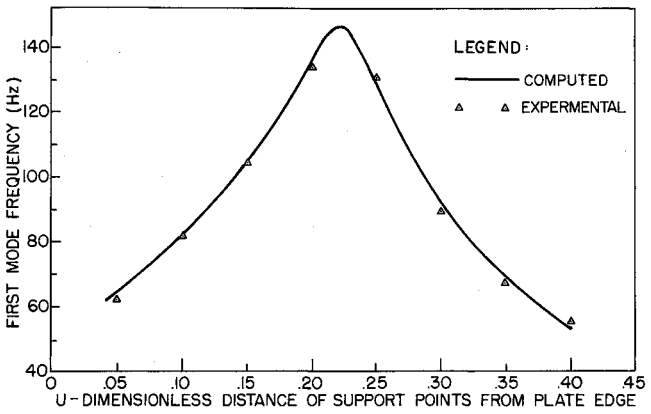

Fig. 7 Comparison of first mode computed and experimentally measured frequencies for plate B.

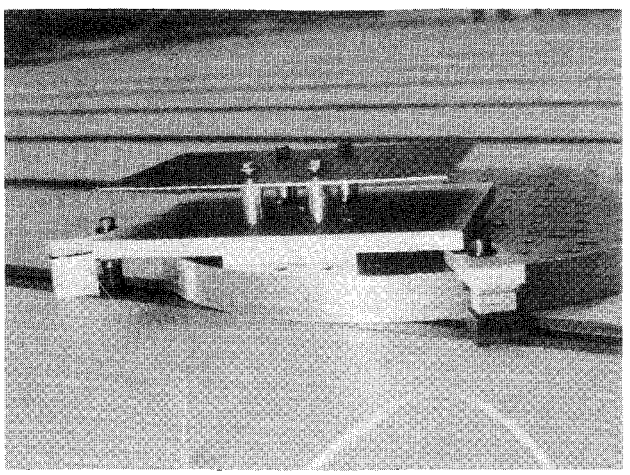

Fig. 8 Photograph of typical test arrangement for measuring resonant frequencies and modes shapes of aluminum plate resting on four rigid point supports.

Figure 9 provides some typical analytical and experimental modes shapes for the first four modes of plate A with supports at $U = 0.15$, whereas Fig. 10 shows the modes shapes of plate B with supports at $U = 0.20$.

Discussion and Conclusions

The rather remarkable ability of the analysis described herein to model rigid point-supported plates becomes strikingly evident upon examining the comparisons between experimental and theoretical results provided. This agreement is particularly well demonstrated in Figs. 6 and 7. The ability of

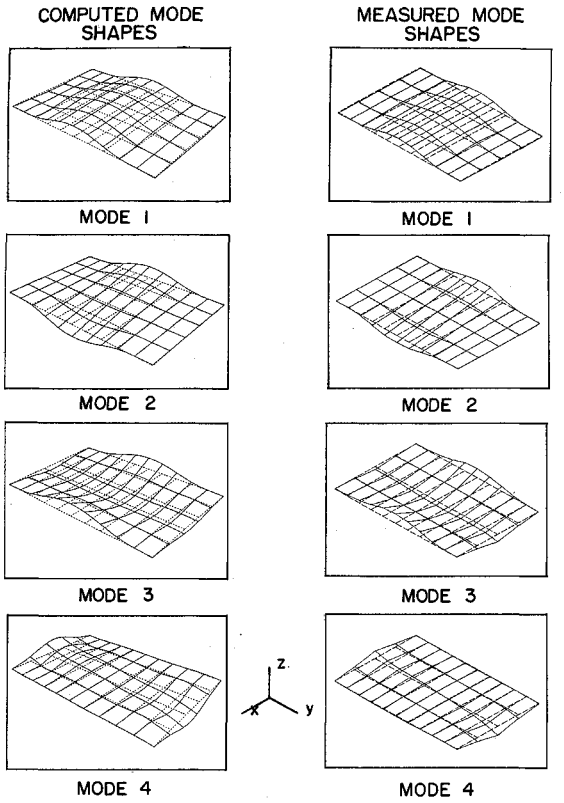

Fig. 9 Comparison of computed and experimentally measured mode shapes for first four modes of plate A with rigid supports dimensionless distance $U = 0.15$ from plate edges.

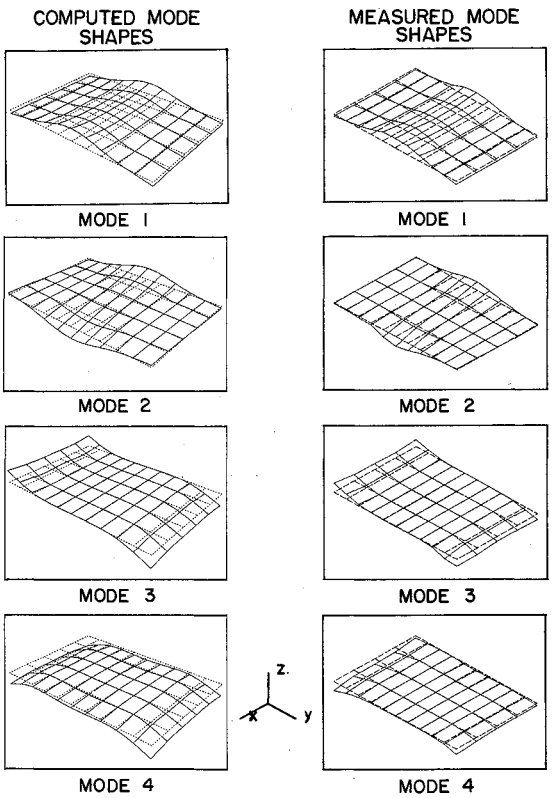

Fig. 10 Comparison of computed and experimentally measured mode shapes for first four modes of plate B with rigid supports dimensionless distance $U = 0.20$ from plate edges.

the analysis to predict mode shapes is well demonstrated in Figs. 9 and 10. It was already known that good agreement between the results of various theoretical studies had been obtained when rectangular plates resting on simple discrete

point supports were studded. This paper demonstrates quite conclusively that employing the superposition method, and simulating rigid point supports with clusters of four discrete point supports, leads to highly accurate results. It is worth recalling that incorporation of each additional rigid point support into the analysis increases the size of the eigenvalue matrix by only four rows and columns, regardless of the number of terms used in the series solutions. Addition of further rigid point supports is therefore easily accommodated in the analysis.

It is shown how the computational procedure can easily be subjected to a minor modification to allow incorporation of the effects of added local masses into the analysis. The general problem of free vibration of rectangular plates resting on rigid point supports and with attached masses will be addressed in a future paper.

The analysis described herein presents the designer with a powerful computational tool that can be used for both the analysis and synthesis of rectangular plate support systems. As indicated earlier, there is a particular interest in plates of the type discussed here in connection with the mounting of solar panels and the support of electronic circuit boards. With this computational tool available, one can not only predict free-vibration frequencies and mode shapes of proposed plate assemblies, one can vary the available parameters to shift the resonant frequencies out of the range where excitation energy is known to be available. It is anticipated, therefore, that the analysis described will play a significant role in future design problems.

Acknowledgments

This work was supported by a grant from the National Sciences and Engineering Research Council of Canada. Experimental work was carried out at the David Florida Laboratory of the Canadian Space Agency in Ottawa, Canada. The authors would also like to acknowledge the technical assistance of H. Ohman, a graduate student at the University of Ottawa.

References

[1]Kerstens, J. G. M., "Vibration of a Rectangular Plate Supported at an Arbitrary Number of Points," *Journal of Sound and Vibration*, Vol. 65, No. 4, 1979, pp. 493–504.

[2]Gorman, D. J., "Free Vibration Analysis of Rectangular Plates with Symmetrically Distributed Point Supports Along the Edges," *Journal of Sound and Vibration*, Vol. 73, No. 4, 1980, pp. 563–574.

[3]Gorman, D. J., "An Analytical Solution for the Free Vibration Analysis of Rectangular Plates Resting on Symmetrically Distributed Point Supports," *Journal of Sound and Vibration*, Vol. 79, No. 4, 1981, pp. 561–574.

[4]Raju, I. S., and Amba-Rao, C. L., "Free Vibrations of Square Plate Symmetrically Supported at Four Points on the Diagonals," *Journal of Sound and Vibration*, Vol. 90, No. 2, 1983, pp. 291–297.

[5]Narita, Y., "Notes on Vibrations of Point Supported Rectangular Plates," *Journal of Sound and Vibration*, Vol. 93, No. 4, 1984, pp. 593–597.

[6]Gorman, D. J., "A Note on the Free Vibration of Rectangular Plates Resting on Symmetrically Distributed Point Supports," *Journal of Sound and Vibration*, Vol. 131, No. 3, 1989, pp. 515–519.

[7]Leuner, T. R., "An Experimental-Theoretical Study of Free Vibrations of Plates on Elastic Point Supports," *Journal of Sound and Vibration*, Vol. 32, No. 4, 1974, pp. 481–490.

[8]Gorman, D. J., *Free Vibration Analysis of Rectangular Plates*, Elsevier-North Holland, New York, 1982.

[9]Gorman, D. J., "Free Vibration of Rectangular Plates with Two Symmetrically Distributed Clamps Along One Edge," *AIAA Journal*, Vol. 24, No. 10, 1986, pp. 1685–1689.